Pure Appl. Chem., Vol. 75, No. 8, pp. 1021–1030, 2003.

Photochemical processes in photosynthesis studied by advanced electron paramagnetic resonance techniques*

Wolfgang Lubitz

Max-Planck-Institut für Strahlenchemie, Stiftstrasse 34-36, D-45470 Mülheim/Ruhr, Germany

Abstract: Various continuous-wave and pulse electron paramagnetic resonance (EPR) and electron nuclear double resonance (ENDOR) experiments performed on the radical species occurring in photosynthetic reaction centers of plants and bacteria during light-induced charge separation are reviewed here. Emphasis is placed on time-resolved experiments performed on short-lived intermediate states such as radical pairs and triplet states for which also hyperfine information can be obtained from pulse ENDOR spectroscopy. Detailed insight into the electronic structure of these intermediates and their interaction with the protein environment is now becoming available.

INTRODUCTION

Photosynthetic reaction centers (RCs) are integral membrane proteins that use sunlight to initiate a fast single-electron transfer (ET) across the photosynthetic membrane. This photochemical process generates a potential difference, which drives subsequent electron and proton transfer reactions. These are coupled to enzymatic processes that, in oxygenic photosynthesis, ultimately oxidize water to dioxygen and yield strongly reducing compounds needed for the conversion of CO_2 to carbohydrates [1]. Whereas cyanobacteria, algae, and green plants use two photosystems (PS I and II) and split water, simple green and purple photosynthetic bacteria possess only one RC and perform an anoxygenic photosynthesis.

In all RCs, the cofactors are arranged in two branches. The primary electron donor (P) is a closely related pair of chlorophyll (Chl) or bacteriochlorophyll (BChl) molecules, the acceptors comprise monomeric chlorophylls, pheophytins (Ph), and quinones (Q) in type II RCs, or chlorophylls, quinones and iron–sulfur centers in type I RCs [2]. The structure of PS II is schematically shown in Fig. 1, together with the main cofactors and the ET pathway. This is based on a recent X-ray structure analysis of PS II core complexes [3]. The structure of the RC of purple bacteria [4] is very similar with respect to the electron acceptors, but differs at the electron donor side, where PS II harbors a protein-bound manganese cluster, the locus of photosynthetic water oxidation.

Detailed understanding of the vectorial ET in these RCs and the coupled catalytic processes (e.g., water oxidation) requires knowledge of both the geometrical arrangements and the electronic structures of all cofactors in their protein environment for all stages of the process. Insight into the spatial structures of the bacterial RCs and of PS I and II has been obtained by X-ray crystallography [3–5]. Information on the electronic structure is available from spectroscopy (for a review, see ref. [6]).

*Lecture presented at the XIXth IUPAC Symposium on Photochemistry, Budapest, Hungary, 14–19 July 2002. Other presentations are published in this issue, pp. 999–1090.

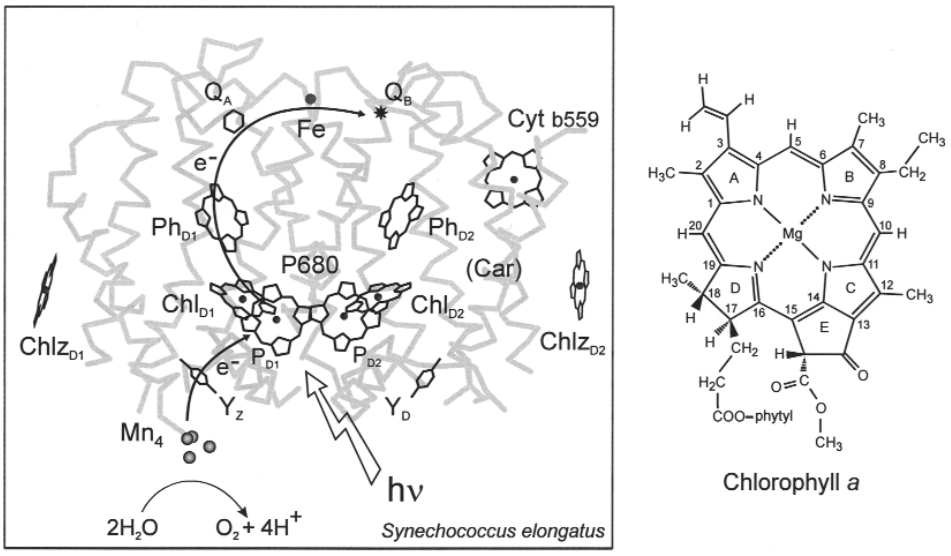

Fig. 1 Cofactor arrangement of PS II core complexes from *Synechococcus elongatus* according to the X-ray crystallographic structure [3]. Cofactors of the central core, P680: pair of Chls (P_{D1}, P_{D2}), monomeric chlorophylls (Chl_{D1}, Chl_{D2}), pheophytins (Ph_{D1}, Ph_{D2}), 2 plastoquinones (Q_A, Q_B), one non-heme Fe^{2+}. The 2 cofactor branches are related by a pseudo-C_2 axis (through P680 and Fe). The arrangement is similar to that of the bacterial RC [4]. Additional cofactors (Chl_Z, cyt b559 heme) are also shown. The light-induced ET path and the coupled water oxidation process (via Y_Z and Mn_4) are indicated schematically. (For details, see text and ref. 3.) The structure of the major pigment Chl *a* is shown on the right; the related BChl *a* has a 3-acetyl group and a 7,8 hydrogenated ring B. (Bacterio)pheophytin is the free base of (B)Chl.

Electron paramagnetic resonance (EPR) is the method of choice to study the transition-metal centers, radical ions, radical pairs, and triplet states occurring in the primary photochemical reactions.

The radicals formed in photosynthetic ET can often be stabilized, and this is a prerequisite for steady-state, continuous-wave (CW) EPR studies [7]. The application of transient and pulse (time-resolved) EPR techniques allows the investigation of short-lived, light-induced intermediate states in the RC [8]. Additional information about the electron-nuclear hyperfine and nuclear quadrupole interaction can be obtained by employing double and triple resonance techniques, such as ENDOR (electron nuclear double resonance) and TRIPLE (electron nuclear triple resonance), both in the CW and pulse modes (for reviews of the techniques used, see [9]). In the following, a few key experiments performed in our laboratory that led to detailed information on these paramagnetic species in the RC, and thus to a better functional understanding of the primary processes in photosynthesis, are described.

RESULTS AND DISCUSSION

Radical ions

In the past, standard CW X-band EPR experiments were primarily used to identify the various radical states in the RC by comparison of *g* values, line widths, and relaxation behavior with those of the isolated cofactor radicals [7]. From the results of EPR experiments, the primary donor in photosynthesis was, for example, identified as a (bacterio)chlorophyll dimer (special pair) [7,10]. With the advent of high-frequency EPR techniques (≥95 GHz), sensitivity and Zeeman resolution could be significantly increased (for a review, see ref. [11]). This has led, for example, to the determination of the full *g* tensor of $P^{+\bullet}$ in single crystals of bRCs [12] and PS I [13], and to a clear distinction of overlapping radical species ($P^{+\bullet}$ and $Q^{-\bullet}$) in the RCs [13]. As an example, the well-resolved W-band EPR spectra of the

two ubiquinone (UQ) radical anions that occur sequentially in the ET in the RC of the purple bacterium *Rhodobacter (Rb.) sphaeroides* are shown in Fig. 2. Although both are UQ-10 molecules, they have quite different spectroscopic and functional properties [14]. The observed difference in *g*-tensor values can be traced back to a different binding situation of the two quinones. $Q_A^{-\bullet}$ is in a more hydrophobic environment than $Q_B^{-\bullet}$, and the H-bonding situation is different (for details, see ref. [14]).

Both quinone radicals can be created simultaneously in the RC yielding the biradical state, $Q_A^{-\bullet}$ $Q_B^{-\bullet}$ [15]. Here, the two electron spins interact via dipolar and exchange interaction, which leads to a splitting of the respective *g*-tensor principal values (Fig. 2, top). Evaluation of the dipolar coupling has led to a detailed picture of the distance between and relative orientations of $Q_A^{-\bullet}$ and $Q_B^{-\bullet}$ in the RC [15]. This result is in very good agreement with the X-ray crystallographic structure of the same RC obtained in the charge-separated state [16]. The measured exchange coupling J is directly related to the electronic matrix element important for the ET process between the two quinones and allows an estimation of the respective ET rate [15].

In the CW EPR spectra, the electron-nuclear hyperfine couplings (HFCs) of the cofactor radicals are often not resolved. Therefore, pulse EPR (electron spin echo envelope modulation, ESEEM) [9] and ENDOR and TRIPLE methods [9] are used to determine the HFCs in solution or single-crystal samples. After assignment of the HFCs to individual nuclei by isotope labeling, a map of the electron spin density distribution in the valence orbital is obtained, which can be compared with theoretical estimates [17,18]. This approach has been used to determine the spin densities of many radical ions that occur in the RCs, see refs. [14,19,20] for examples. Furthermore, the dipolar HFCs contain information about the geometrical structure (e.g., hydrogen-bond lengths) between the cofactors and the protein that can be probed [14].

The HFCs are sensitive probes for variations of the pigment structures or their interaction with each other or with their environment. We have studied the impact of the protein on structure and function of the embedded cofactors. Specific mutants were constructed that changed the metal ligation, hy-

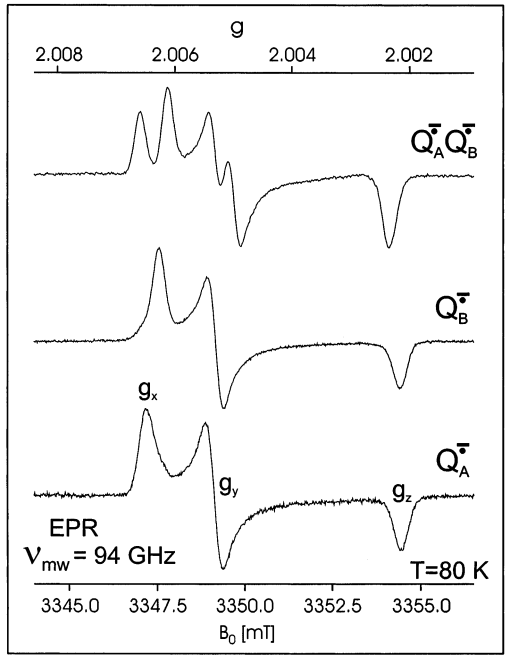

Fig. 2 W-band EPR spectra of $Q_A^{-\bullet}$ and $Q_B^{-\bullet}$, and the biradical state $Q_A^{-\bullet}$ $Q_B^{-\bullet}$ in deuterated ZnRCs of *Rb. sphaeroides* (frozen solution). The principal g tensor components $g_{x,y,z}$ are indicated; for details, see refs. [14,15].

drogen-bonding to carbonyl groups, or the conformation of the cofactors. In the case of the primary donor in *Rb. sphaeroides*, the replacement of histidine (H), ligating the central Mg of the BChls, with bulky amino acids such as leucine (L) or glutamate (E) leads to a loss of the metal ion, and a different dimeric species (a BChl-BPh-heterodimer) is formed with different spin density distribution, midpoint potential (E_m), and functional properties [21]. In the respective mutant HE(M202), the electron spin distribution is very close to that of monomeric BChl $a^{+\bullet}$, the E_m values are also similar (see Fig. 3), and the ET rate is reduced compared to wild type. The donor actually acts like a monomeric species. This mutant clearly shows that Nature has used a dimeric chlorophyll in the native RC to significantly lower and thereby adjust the donor's redox potential for optimum ET in the RC. At the same time, the optical properties for proper overlap with the antenna system are adjusted by exciton splitting. Changes of the H bonds between the protein and the primary donor also led to large changes of the spin distribution in the dimer, the oxidation potentials, and various ET rates in the RC [22,23]. A correlation between the electronic and redox properties of these mutants enabled us to shed light on the question of how the amino acid surrounding tunes the embedded cofactors for optimum function in the RC [24].

In the bacterial RC, and also in PS I, the primary donors have been identified as (B)Chl-dimers [4,5] and the EPR/ENDOR results have shown that the unpaired electron, and thus the positive charge, is (asymmetrically) distributed in a supermolecular orbital extending over both dimer halves [19,20,25,26]. As described above, dimer formation leads to a decrease of the oxidation potential owing to the increased charge delocalization and stabilization of $P^{+\bullet}$. Whereas in these reaction centers, a low

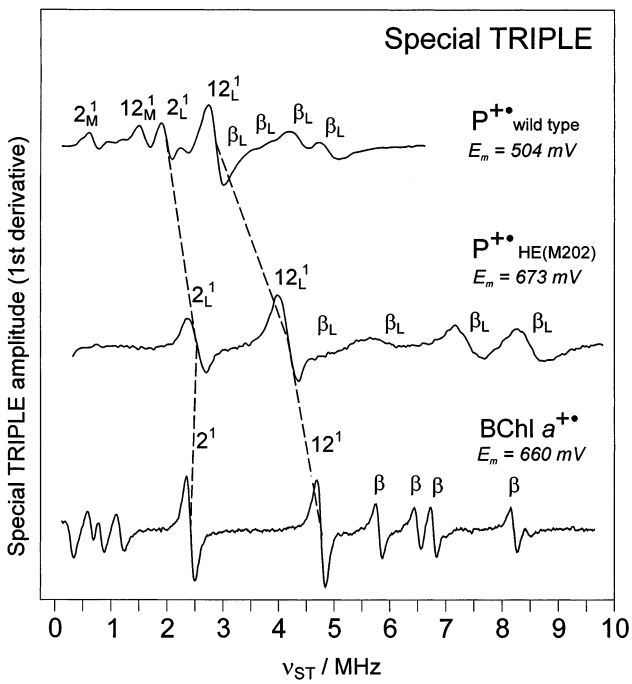

Fig. 3 Electron-nuclear-nuclear TRIPLE resonance spectra of the primary donor cation radical $P^{+\bullet}$ in RCs of *Rb. sphaeroides* wild-type and mutant HE(M2O2), in which one histidine ligand to the BChl-dimer is replaced by glutamate (see text); the spectrum of monomeric BChl $a^{+\bullet}$ in organic solvent is shown for comparison (all spectra in isotropic liquid solution). The midpoint potentials E_m (P/P^+) and E_m ($BChl/BChl^+$) are also given. The HFCs are directly obtained from the TRIPLE frequency ν_{ST} ($A_{iso} = 2\nu_{ST}$). For assignments, see molecular structure in Fig. 1 (β denotes the hydrogens on rings B and D, the two dimer halves of P are denoted by L and M). For further details, see ref. [21].

potential of the electron donors is necessary for optimum ET and proper coupling to secondary reactions, in PS II a midpoint potential high enough for water oxidation is required. Estimates show that $E_m(P/P^+)$ lies at about +1.2 V in PS II. This makes the dimeric Chl species unlikely to act as the primary donor in PS II. It is very difficult to stabilize and study this highly reactive species since several secondary electron donor pathways exist in PS II, which can lead to the oxidation of other cofactors. Among the several possible secondary donors to P^+, carotenoid (Car), chlorophyll (Chl_Z), and Cyt b_{559} have been discussed [27] (see Fig. 1).

The papers reporting on EPR/ENDOR studies of $P^{+\bullet}$ in special PS II samples show that the species observed is rather a (perturbed) monomeric Chl $a^{+\bullet}$ than a dimeric species [28,29]. It is, however, not entirely clear on which pigment the electron spin is actually located in these preparations. The proposal of a monomeric Chl acting as the primary donor in PS II is supported by the X-ray crystallographic structure that shows rather large center-to-center distances ($\gtrsim$10 Å) for all chlorophyll pigments of the PS II RC core [3] in contrast to the situation found in PS I [5] and bRC [4].

The quinone acceptors in the bRC have been studied by similar techniques [14]. The measured hf data clearly show that the binding site of Q_A is strongly asymmetric, which is in contrast to that of the secondary quinone, Q_B. Hydrogen bonds of different strength, which were directly detected by ENDOR, are probably mainly responsible for this difference. Application of ESEEM to $Q_A^{-\bullet}$ and $Q_B^{-\bullet}$ revealed the interaction of both radicals with nitrogen nuclei. The measured ^{14}N nuclear quadrupole couplings served to identify these nuclei with certain amino acid residues [30,31]. The obtained ^{14}N HFCs indicate delocalization of the electronic wave function carrying the unpaired electron onto the surrounding amino acids—probably via the H bonds. This finding has important implications for the mechanism of ET. Similar studies have been reported for $A_1^{-\bullet}$ in PS I [32] and $Q_A^{-\bullet}$ in PS II [33].

Radical pairs

In the charge-separation process, radical pairs (RPs) of the donor and the acceptors are formed, which can be observed by time-resolved (transient) EPR spectroscopy [8]. The method uses "direct detection" and achieves a time resolution of a few ns. Owing to the high spin polarization of the initial charge-separated state, a strongly increased sensitivity is obtained. In the time window (ns to μs), detection of several RP states in the various RCs is possible (see Table 1). A simulation of the spin-polarized spectra allows the determination of the relative orientation of the radicals and, with lesser accuracy, of the distance. Such spectra have also been obtained from single crystals at higher microwave frequencies

Table 1 Comparison of cofactor distances determined by out-of-phase ESEEM on radical pairs and X-ray crystallography.

	RP	r (EPR)/Å	R (X-ray)/Å
Rb. sphaeroides[a]	$P_{865}^{+\bullet}\,Q_A^{-\bullet}$	28.4 ± 0.3	28.3
Rps. viridis[b]	$P_{960}^{+\bullet}\,Q_A^{-\bullet}$	28.8 ± 0.3	28.1
PS II[c]	$P_{680}^{+\bullet}\,Q_A^{-\bullet}$	27.4 ± 0.3	26/28[e]
PS II[c]	$Y_Z^{ox}\,Q_A^{-\bullet}$	34 ± 1	33.5[f]
PS I[d]	$P_{700}^{+\bullet}\,A_1^{-\bullet}$	25.4 ± 0.3	26.0[g]

[a][35,37]
[b][41]
[c][42]
[d][35]
[e]For P_{D1}/P_{D2} (Fig. 1), respectively, see ref. [3].
[f][3]
[g][5]

(35 GHz) [13], which yield additional information on the interaction parameters. The extension to W-band (95 GHz) [34] allowed a complete separation of the two radicals in the RP and thus provided very accurate structural data, see, e.g., ref. [13].

A precise determination of the distance between radical centers in the RP is possible by application of pulse EPR techniques (out-of-phase ESEEM) as described in [35,36]. Table 1 shows distances measured by this method in two bacterial RCs, PS I and II. The data agree well with those derived from the X-ray structures. In PS II, this comparison clearly shows that the cationic state is located on the time scale of the experiment (ns to μs), on P_{D1} (or P_{D2}) before the donor cation is reduced by tyrosine Y_Z (cf. Fig. 1).

The EPR techniques described above can be used advantageously to detect light-induced structural changes in the RC. Such changes had been observed for the ET rates when RCs were either frozen in the dark and then illuminated or frozen in the light, i.e., in the charge-separated state (see ref. [37] for refs.). Such experiments using pulse and transient EPR applied to the RP state, $P_{865}^{+\bullet}\ Q_A^{-\bullet}$, in *Rb. sphaeroides* have already been reported [37,38].

Recently, Bittl et al. [39,50] showed that pulse ENDOR experiments can also be performed on short-lived, spin-polarized RP states. This opens the possibility of detecting the HFCs of the two radicals on a μs-time scale directly after charge separation before a major structural relaxation occurs. Figure 4 shows a comparison of the ENDOR spectra performed on the spin-polarized RP ($P_{700}^{+\bullet}\ A_1^{-\bullet}$) and the photo-accumulated phylloquinone radical anion $A_1^{-\bullet}$ in frozen PS I particles. It would be interesting to perform such experiments also on $P^{+\bullet}\ Q_A^{-\bullet}$ in PS II to directly detect the HFCs of $P_{D1}^{+\bullet}$ (see above); data for $Q_A^{-\bullet}$ in PS II have been obtained earlier [40].

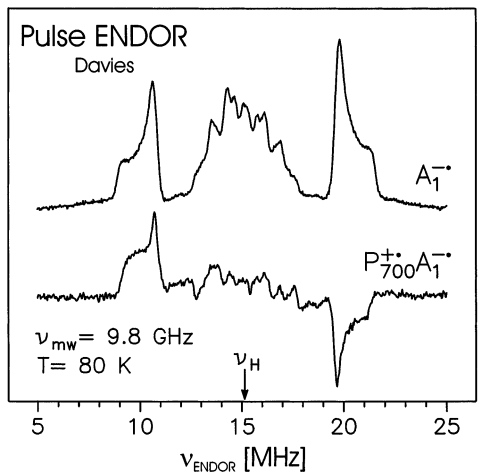

Fig. 4 Pulse ENDOR spectra of the photoaccumulated radical anion of the primary quinone acceptor $A_1^{-\bullet}$ and the spin-polarized radical pair state $P_{700}^{+\bullet}\ A_1^{-\bullet}$ in PS I. For details, see refs. [39,50].

Photoexcited triplet states

The triplet state of the primary donor ^3P can be generated via radical pair recombination in prereduced RCs in which forward ET past the primary RP is blocked. ^3P has a short lifetime (0.1–1 ms) and yields a strongly spin-polarized transient EPR spectrum (Fig. 5, top) from which the zero field splitting parameters *D* and *E* are available [43]. Until recently, very little was known about the hyperfine structure of such triplet species. Lendzian et al. have applied Davies pulse ENDOR to ^3P in bacterial RCs (^{3}P865) [44] and also in plant PS II preparations (^{3}P680) [45,51]. The data were compared with those from ^{3}BChl *a* and ^{3}Chl *a*, respectively, in frozen organic glasses. The results clearly showed that the triplet

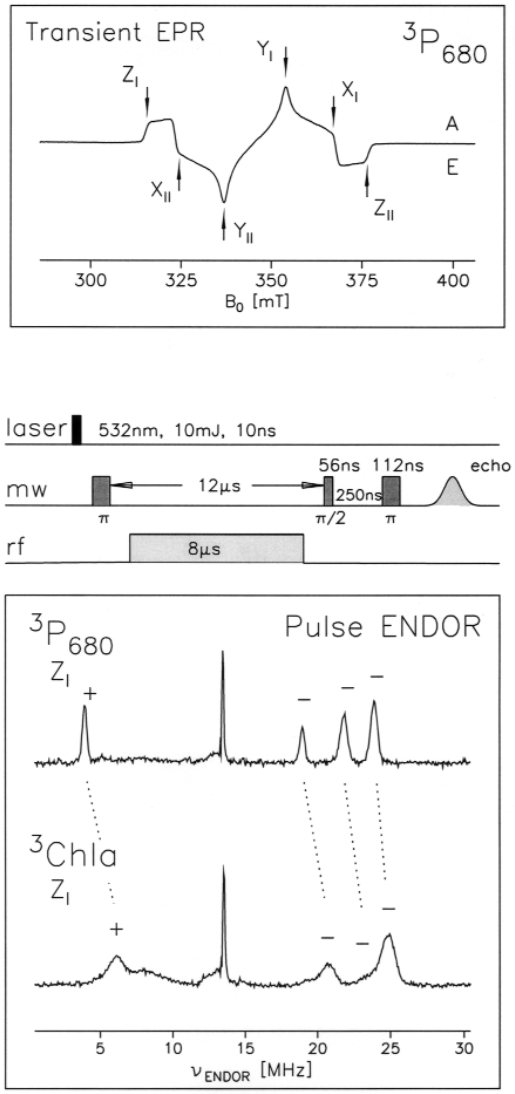

Fig. 5 Spin-polarized transient EPR of ^{3}P680 in PS II at X-band, T = 10 K (top); Pulse ENDOR of ^{3}P680 in PS II and ^{3}Chl *a* (organic solvent) at 10 K obtained at EPR position Z_I (bottom); the pulse ENDOR scheme is also given (center), for details, see refs. [21,44,45,51].

exciton is *delocalized* over a BChl dimer in the case of ^{3}P865, and *localized* on a monomeric Chl in ^{3}P680 in PS II (see also discussion in ref. [43]). It has been proposed from EPR experiment on ^{3}P in oriented PS II membrane fragments and a comparison with the bRC that this triplet state is not localized on a Chl of the "special pair" (P_{D1}/P_{D2} in Fig. 1) but on an accessory chlorophyll [46]. We have very recently completed a transient EPR study on ^{3}P in prereduced PS II single crystals at low temperatures [47]. The analysis of the orientation-dependent EPR spectra yielded the precise magnitude and axes orientation of the ZFS tensor in PS II. It was found that D_z, which is oriented perpendicular to the chlorophyll π-plane, forms an angle of 30 ± 2° with the pseudo-C_2 axes of the PS II RC, which runs through the pair of chlorophylls P_{D1}/P_{D2} and the non-heme Fe (Fig. 1); this C_2 axis is parallel to the membrane normal. The result fully supports the earlier proposal that the triplet state is *not* localized on

P_{D1} or P_{D2}, but on one of the monomeric chlorophylls. According to the crystal structure, it is localized on either Chl_{D1} or Chl_{D2}, their plane normals form an angle of ~29° with the C_2 axis [3]. Furthermore, the analysis of the single-crystal experiments, together with some structural information from ENDOR, allowed the determination of the position of the in-plane axes D_x and D_y of the ZFS tensor and thus a full positioning of the Chl ring in the PS II crystal structure [47]. It turned out that the orientation of the individual chlorophylls is similar to those in the bRC [4].

These results show that in PS II, at least on a microsecond time scale, the positive charge and the triplet exciton are *not* located on the same molecule in contrast to the bRC [48]. Recently, Diner et al. [49] arrived at the same conclusion based on the analysis of optical data. It can be speculated that this indicates also a possible difference of the charge-separation processes in bacterial RCs and PS II [47,49,52].

CONCLUSION

EPR techniques applied to paramagnetic functional intermediates in photosynthetic RCs proved to be very useful for determining relative orientations, distances and electronic structures of these species as well as their interaction with the protein environment. Furthermore, EPR parameters are sensitive probes for structural changes occurring in the process of light-induced charge separation. Correlation with other physical properties (e.g., redox potentials and kinetic data) helped to understand the function of the cofactors in the protein and yielded insight into the primary process of photosynthesis in general [21].

ACKNOWLEDGMENTS

The author thanks all coworkers and colleagues who contributed to this work and whose names are given in the cited references. The work was supported by DFG (Sfb 498 and Priority Program SPP 1051), European Union (FMRX-CT 98-0214), and Fonds der Chemischen Industrie (Germany).

REFERENCES

1. D.-P. Häder. *Photosynthese*, Georg Thieme, Stuttgart (1999).
2. W.-D. Schubert, O. Klukas, W. Saenger, H. T. Witt, P. Fromme, N. Krauß. *J. Mol. Biol.* **280**, 297 (1998).
3. A. Zouni, H. T. Witt, J. Kern, P. Fromme, N. Krauß, W. Saenger, P. Orth. *Nature* **409**, 73 (2001).
4. C. R. D. Lancaster, U. Ermler, H. Michel. In *Anoxygenic Photosynthetic Bacteria*, R. E. Blankenship, M. T. Madigan, C. E. Bauer (Eds.), Vol. 2, pp. 503–526, Kluwer, Dordrecht (1995).
5. P. Jordan, P. Fromme, H. T. Witt, O. Klukas, W. Saenger, N. T. Krauß. *Nature* **411**, 909 (2001).
6. A. J. Hoff and J. Deisenhofer. *Phys. Rep.* **287**, 1 (1997).
7. G. Feher and M. Y. Okamura. In *The Photosynthetic Bacteria*, Clayton & Sistrom, (Eds.), p. 349, Plenum, New York (1978).
8. D. Stehlik and K. Möbius. *Annu. Rev. Phys. Chem.* **48**, 745 (1997).
9. J. Amesz and A. J. Hoff (Eds.). *Biophysical Techniques in Photosynthesis*, Chaps. 14–16, Kluwer, Dordrecht (1996).
10. J. R. Norris, R. A. Uphaus, H. L. Crespi, J. J. Katz. *Proc. Natl. Acad. Sci. USA* **68**, 625 (1971).
11. K. Möbius. *Chem. Soc. Rev.* **29**, 129 (2000).
12. R. Klette, J. T. Törring, M. Plato, K. Möbius, B. Bönigk, W. Lubitz. *J. Phys. Chem.* **97**, 2015 (1993).
13. S. Zech, W. Hofbauer, A. Kamlowski, P. Fromme, D. Stehlik, W. Lubitz, R. Bittl. *J. Phys. Chem. B* **104**, 9728 (2000); C. Teutloff, W. Hofbauer, S. Zech, R. Bittl, W. Lubitz. *Appl. Magn. Res.* **21**, 363 (2001).

14. W. Lubitz and G. Feher. *Appl. Magn. Res.* **17**, 1 (1999).
15. R. Calvo, E. C. Abresch, R. Bittl, G. Feher, W. Hofbauer, R. A. Isaacson, W. Lubitz, M. Y. Okamura, M. L. Paddock. *J. Am. Chem. Soc.* **122**, 7327 (2000); R. Calvo, R. Isaacson, M. Paddock, E. Abresch, M. Okamura, A. L. Maniero, L. C. Brunel, G. Feher. *J. Phys. Chem. B* **105**, 4053 (2001).
16. H. Stowell, T. McPhillips, D. Rees, S. Soltis, E. Abresch, G. Feher. *Science* **276**, 812 (1997).
17. M. Plato, K. Möbius, W. Lubitz. In *Chlorophylls*, H. Scheer (Ed.), pp. 1015–1046, CRC Press, Boca Raton, FL (1991).
18. S. Sinnecker, W. Koch, W. Lubitz. *Phys. Chem. Chem. Phys.* **2**, 4772 (2000); S. Sinnecker, W. Koch, W. Lubitz. *J. Phys. Chem. B* **106**, 5281 (2002).
19. F. Lendzian, M. Huber, R. A. Isaacson, B. Endeward, M. Plato, B. Bönigk, K. Möbius, W. Lubitz, G. Feher. *Biochim. Biophys. Acta* **1183**, 139 (1993).
20. H. Käß, P. Fromme, H. T. Witt, W. Lubitz. *J. Phys. Chem. B* **105**, 1225 (2001).
21. W. Lubitz, F. Lendzian, R. Bittl. *Acc. Chem. Res.* **35**, 313 (2002).
22. J. Rautter, F. Lendzian, C. Schulz, A. Fetsch, M. Kuhn, X. Lin, J. C. Williams, J. P. Allen, W. Lubitz. *Biochemistry* **34**, 8130 (1995).
23. J. P. Allen and J. C. Williams. *J. Bioenerg. Biomembr.* **27**, 275 (1995).
24. F. Müh, F. Lendzian, J. C. Williams, J. P. Allen, W. Lubitz. *J. Phys. Chem. B* **106**, 3226 (2002).
25. A. N. Webber and W. Lubitz. *Biochim. Biophys. Acta* **1507**, 61 (2001).
26. H. Witt, E. Schlodder, C. Teutloff, J. Niklas, E. Bordignon, D. Carbonera, S. Kohler, A. Labahn, W. Lubitz. *Biochemistry* **41**, 8557 (2002).
27. J. Hanley, Y. Deligiannakis, A. Pascal, P. Faller, A. W. Rutherford. *Biochemistry* **38**, 8189 (1999).
28. S. E. J. Rigby, J. H. A. Nugent, P. J. O'Malley. *Biochemistry* **33**, 10043 (1994).
29. A. Telfer, F. Lendzian, E. Schlodder, J. Barber, W. Lubitz. In *Photosynthesis: Mechanisms and Effects*, G. Garab (Ed.), Vol. II, pp. 1061–1064, Kluwer, Dordrecht (1998).
30. M. K. Bosch, P. Gast, A. J. Hoff, A. P. Spoyalov, Yu. D. Tsvetkov. *Chem. Phys. Lett.* **239**, 306 (1995).
31. F. Lendzian, J. Rautter, H. Käß, A. Gardiner, W. Lubitz. *Ber. Bunsen-Ges. Phys. Chem.* **100**, 2036 (1996).
32. J. H. Hanley, Y. Deligiannakis, F. MacMillan, H. Botin, A. W. Rutherford. *Biochemistry* **36**, 11543 (1997).
33. Y. Deligiannakis, J. Hanley, A. W. Rutherford. *J. Am. Chem. Soc.* **121**, 7653 (1999).
34. T. F. Prisner, A. van der Est, R. Bittl, W. Lubitz, D. Stehlik, K. Möbius. *Chem. Phys.* **194**, 361 (1995).
35. R. Bittl and S. G. Zech. *J. Phys. Chem. B* **101**, 1429 **(**1997).
36. S. A. Dzuba and A. J. Hoff. In *Biological Magnetic Resonance*: *Distance Measurements in Biological Systems by EPR*, L. J. Berliner, S. S. Eaton, G. R. Eaton (Eds.), Chap. 13, Kluwer Academic/Plenum, New York (2000).
37. S. Zech, R. Bittl, A. Gardiner, W. Lubitz. *Appl. Magn. Res*. **13**, 517 (1997).
38. I. V. Borovykh, S. A. Dzuba, I. I. Proskuryakov, P. Gast, A. J. Hoff. *Biochim. Biophys. Acta* **1363**, 182 (1998).
39. R. Bittl, S. G. Zech, C. Teutloff, L. Krabben, W. Lubitz. In *Photosynthesis: Mechanisms and Effects*, G. Garab (Ed.), Vol. I, p. 509, Kluwer, Dordrecht (1998).
40. F. MacMillan, F. Lendzian, G. Renger, W. Lubitz. *Biochemistry* **34**, 8144 (1995).
41. A. T. Gardiner, S. G. Zech, F. MacMillan, H. Käß, R. Bittl, E. Schlodder, F. Lendzian, W. Lubitz. *Biochemistry* **38**, 11773 (1999).
42. S. G. Zech, J. Kurreck, G. Renger, W. Lubitz, R. Bittl. *FEBS Lett.* **442**, 79 (1999).
43. D. E. Budil and M. C. Thurnauer. *Biochim. Biophys. Acta* **1057**, 1 (1991).
44. F. Lendzian, R. Bittl, W. Lubitz. *Photosyn. Res.* **55**, 189 (1998).

45. F. Lendzian, R. Bittl, A. Telfer, J. Barber, W. Lubitz. In *Photosynthesis: Mechanisms and Effects*, G. Garab (Ed.), Vol. II, p. 1057, Kluwer, Dordrecht (1998).
46. F. J. E. van Mieghem, K. Satoh, A. W. A. Rutherford. *Biochim. Biophys. Acta* **1058**, 379 (1991).
47. M. Kammel, J. Kern, W. Lubitz, R. Bittl. *Biochim. Biophys. Acta* (2003). In press.
48. J. R. Norris, D. E. Budil, P. Gast, C.-H. Chang, O. El-Kabbani, M. Schiffer. *Proc. Natl. Acad. Sci. USA* **86**, 4335 (1989).
49. B. A. Diner, E. Schlodder, P. J. Nixon, W. J. Coleman, F. Rappaport, J. Lavergne, W. F. J. Vermaas, D. A. Chisholm. *Biochemistry* **40**, 9265 (2001).
50. C. E. Fursman, Ch. Teutloff, R. Bittl. *J. Phys. Chem. B* **106**, 9679 (2002).
51. F. Lendzian, R. Bittl, A. Telfer, W. Lubitz. *Biochim. Biophys. Acta* (2003). In press.
52. W. Lubitz. *Phys. Chem. Chem. Phys.* **4**, 5539 (2002).